

pubs.acs.org/joc Article

Switching a HO $\cdots\pi$ Interaction to a Nonconventional OH $\cdots\pi$ Hydrogen Bond: A Completed Crystallographic Puzzle

Muhammad Kazim, Liangyu Guan, Anant Chopra, Roy Sun, Maxime A. Siegler, and Thomas Lectka*



Cite This: https://dx.doi.org/10.1021/acs.joc.0c01121



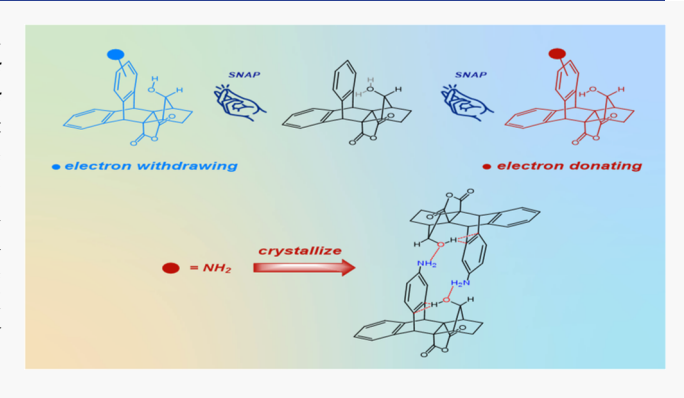
ACCESS

III Metrics & More



s Supporting Information

ABSTRACT: In this article, we present crystallographic and spectroscopic evidence of a tunable system wherein a $HO\cdots\pi$ interaction switches incrementally to a nonconventional $OH\cdots\pi$ hydrogen bonding (HB) interaction. More specifically, we report the synthesis of substituted forms of model system 1 to study the effects of aryl ring electronic density on the qualitative characteristics of $OH\cdots\pi$ hydrogen bonds therein. The OH stretch in experimental infrared data, in agreement with density-functional theory (DFT) calculations, shows continuous red-shifts as the adjacent ring becomes more electron rich. For example, the OH stretch of an amino-substituted analogue is red-shifted by roughly $50~{\rm cm}^{-1}$ compared to the same stretch in the CF_3 analogue, indicating a significantly stronger HB interaction in the former.



Moreover, DFT calculations (ω B97XD/6-311+G**) predict that increasing electronic density on the adjacent *top* ring reduces the aryl π -OH σ^* energy gap with a concomitant enhancement of the OH n- π^* energy gap. Consequently, a dominant π - σ^* interaction in the amino substituted analogue locks the system in the *in*-form while a favorable n- π^* interaction reverses the orientation of the oxygen-bound hydrogen in its protonated form. Additionally, the ¹H NMR data of various analogues reveal that stronger OH··· π interactions in systems with electron-rich aromatic rings slow exchange of the alcoholic proton, thereby revealing coupling with the geminal proton. Finally, X-ray crystallographic analyses of a spectrum of analogues clearly visualize the three distinct stages of "switch"—starting with exclusive HO··· π , to partitioned HO··· π /OH··· π , and finally to achieving exclusive OH··· π forms. Furthermore, the crystal structure of the amino analogue reveals an interesting feature in which an extended HB network, involving two conventional (NH···O) and two nonconventional (OH··· π) HBs, dimerizes and anchors the molecule in the unit cell.

■ INTRODUCTION

Nonconventional hydrogen bonds between X–H, where X is an electronegative atom, and the π cloud of an aromatic ring (Figure 1) have significant importance in chemistry and







nonconvention H-bond

Figure 1. Generic $HO\cdots\pi$ and $OH\cdots\pi$ rotameric forms leading to through space arene activation and a nonconventional H-bonding interaction.

structural biology.^{1–10} For example, Steiner and Koellner screened a list of 529 high-resolution protein crystal structures and noted that one in almost 11 protein residues with aromatic side chains act as π -hydrogen bond acceptors.¹¹ Additionally, several examples of small molecules depicting such interactions are reported in the literature.^{12–20} Nonetheless, many aspects of these intriguing noncovalently bonded interactions remain

relatively unexplored. We thought it is important to construct a rigid molecular system exhibiting close yet tunable $OH\cdots\pi$ hydrogen bonding (HB) properties, in order to establish a more detailed understanding of this timely problem. In this regard, we report the syntheses of a few substituted analogues based on the fused 9,10-dihydroanthracene-bicycloheptane scaffold (e.g. compound 1) that facilitate a more thorough investigation of nonconventional $OH\cdots\pi$ hydrogen bonds (Figure 2). Most importantly, these analogues permitted us to characterize three distinct geometric stages of interaction: the exclusive $HO\cdots\pi$, the partitioned $HO\cdots\pi/OH\cdots\pi$, and the exclusive $OH\cdots\pi$.

Our previous analysis of compound 1 focused on the fortuitous $HO\cdots\pi$ interaction that resulted in a strong through-

Received: May 8, 2020 Published: July 7, 2020



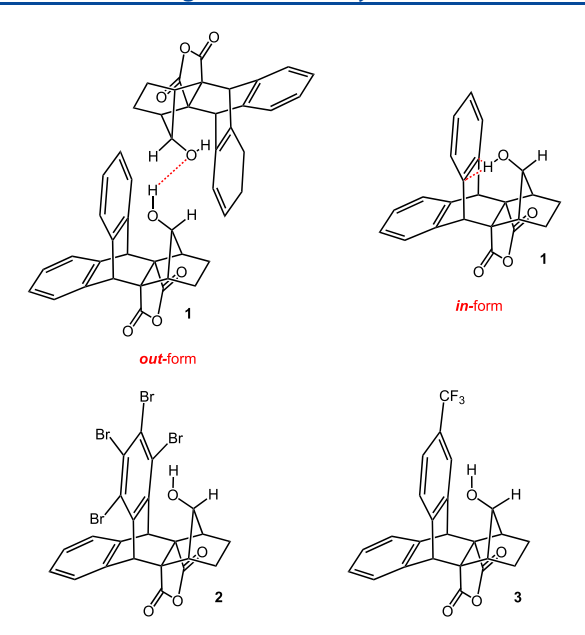


Figure 2. Structures of compounds 1 (the *in*-form engages in nonconventional HB while the *out*-form engages in a conventional HB), 2, and 3.

space activation of the adjacent "top" ring toward electrophilic aromatic substitution reactions. However, crystallographic analysis of compound 1 revealed that the oxygen-bound hydrogen atom is partitioned between two orientations. In the *in*-form, it engages in a nonconventional OH··· π hydrogen bond with the top ring's π system (OH···C_{aryl} distance = 2.03 Å), whereas in the *out*-form it engages in a conventional OH··· π O hydrogen bond with an oxygen atom of a neighborium molecule (OH···O distance = 1.94 Å) (Figure 2). Furthermore, when the *top* ring was functionalized with deactivating groups, the oxygen-bound hydrogen could no longer benefit from a strong OH··· π hydrogen bond. For example, in the crystal structure of tetrabrominated analogue 2, the oxygen-bound hydrogen was exclusively locked in the *out*-form (Figure 2). Late of the structure of tetrabrominated analogue 2, the oxygen-bound hydrogen was exclusively locked in the *out*-form (Figure 2).

It is important to note that the $OH\cdots\pi$ distance observed in the *in*-form of **1** is very close to the shortest such distance established crystallographically (1.98 Å).²² Therefore, this observed nonconventional hydrogen bond could be classified as one of the stronger $OH\cdots\pi$ interactions. However, none of the molecules reported in our previous article exhibited the oxygen-bound hydrogen to be locked exclusively in the *in*-form to allow a more extensive investigation of this phenomenon.

It has been suggested that stronger hydrogen bonds have more covalent character, whereas weaker hydrogen bonds are dominated by electrostatic interactions. Boxer and coworkers established a direct correlation between the electronic nature of the aromatic ring and the strength of various π -hydrogen bonds in solution employing substituted benzene complexes. Their results indicate that the electrostatic properties of the hydrogen bond acceptor, namely the aromatic ring, dominate these interactions in solution. He imagined that an electron-rich analogue of compound 1 might benefit from a significantly stronger $OH \cdots \pi$ hydrogen bond and thus lock the system in the *in*-form, thus providing the missing "third stage".

RESULTS AND DISCUSSION

To test this hypothesis, we turned to density-functional theory (DFT) calculations (ω B97XD/6-311+G**). The *in*-form is predicted to be favored by 6.7 kcal/mol when the *top* ring is substituted by an amino group. Similarly, in molecule 1 (R = H), the *in*-form is predicted to be 5.8 kcal/mol more stable than the *out*-form (gas phase), in part due to favorable OH··· π interactions. However, in the *top*-CF₃ analogue (compound 3, Figure 2), the *in* and *out* forms are predicted to be almost isoenergetic (Figure 3). This apparent drop in selectivity can

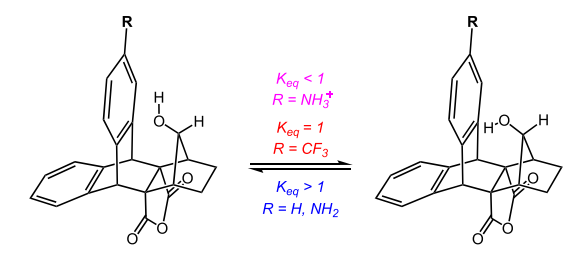


Figure 3. Isodesmic relation comparing the energies of in and out rotamers (DFT— ω B97XD/6-311+ G^{**}); R = NH₃⁺, CF₃, H, NH₂.

be attributed to less propitious $OH\cdots\pi$ interactions in an electron-poor system. On the other hand, we imagined that a protonated amino analogue might switch the rotameric preference as the substituent becomes an electron withdrawing group $(-NH_3^+ \text{ vs } -NH_2)$. When optimized $(\omega B97XD/6-311+G^{**})$, the *out*-form of top NH_3^+ analogue is predicted to be more stable by roughly 10 kcal/mol compared to the respective *in*-form, indicating a protonation-driven switch from a favorable $OH\cdots\pi$ hydrogen bond in the NH_2 derivative to a complete $HO\cdots\pi$ interaction in the NH_3^+ version (Figure 3).

After DFT calculations pointed us in the right direction, we embarked upon the synthesis of the *top*-NH₂ analogue 5. Subjecting 1 to nitrating conditions results in exclusive formation of 4 (Scheme 1). Formation of the nitrate ester is

Scheme 1. Synthesis of Compound 5

evident from ¹H NMR, wherein the hydroxyl proton disappears in the product and the proton on C1 appears deshielded at 4.72 ppm in 4 (-0.22 and 3.85 ppm, respectively, in 1). Hydrogenation at 3 atm simultaneously clove the nitrate ester and reduced the aromatic nitro group to generate the target molecule 5 (Scheme 1).

Infrared Spectroscopic Analysis. We envisioned that infrared (IR) spectroscopy would be a critical tool in the investigation of this system. Generally speaking, increasing the strength of a classical hydrogen bond results in lengthening of the donor—H bond and a concomitant shortening of the acceptor···H distance, thereby inducing a lower energy shift in the respective IR-stretching frequency. Compounds 1, 3 (top CF_3 analogue), and 5 were considered; initial DFT analysis at ω B97XD/6-311+G** predicts increasing red-shifts of the OH stretching frequencies of the *in*-forms as the adjacent *top* ring becomes more electron rich (Table 1). As

Table 1. Calculated (Scaled) and Experimentally Observed OH Stretching Frequencies in 1, 3, and 5

OH stretch cm ⁻¹	$R = CF_3$	Н	NH_2
predicted (in forms)	3762	3745	3707
experimental	3606	3578	3553

expected, the *out*-forms show no significant trend in these candidates, as their oxygen bound hydrogen atoms do not engage in $OH\cdots\pi$ interactions (See Supporting Information for details). Experimentally, the IR spectrum of 5 locates an OH stretch at 3553 cm⁻¹ that is red-shifted by roughly 50 and 25 cm⁻¹ compared to the same stretch in 3 and 1.²¹ This observation is congruent with stronger hydrogen bond in 5 (Table 1 and Figure 4). The IR spectrum of 5 also locates the N–H stretch at 3395 cm⁻¹ (consistent with DFT calculations which predict the NH stretch to appear roughly 160 cm⁻¹ less than the OH stretch) (Figure 5, red spectrum).

Interestingly, calculations indicate that the OH stretches of the *in*-forms are affected differently in these molecules depending on the nature of the substituent on the adjacent *top* ring. For example, OH stretches of the *in*-forms are predicted to be "blue"-shifted by 34 cm⁻¹ in 3, almost identical (no shift) in 1 and "red"-shifted by 18 cm⁻¹ in 5 compared to OH stretches in their corresponding *out*-forms. These calculations suggest that electron-deficient rings have a

propensity to induce blue-shifts whereas electron-rich rings can induce red-shifts in OH stretching frequencies.

When compound 5 was subjected to protonation with 1 equiv of 1 M HCl in CH_2Cl_2 , we observed a large blue-shift in the OH stretching region. The OH stretching frequency in 5 (3553 cm⁻¹) shifts to 3685 cm⁻¹, indicating a significantly weaker (probably absent) OH··· π HB interaction in the protonated form (Figure 5). The IR spectrum of 5–H⁺ also locates the NH stretch at 3600 cm⁻¹ (predicted 3707 and 3605 cm⁻¹ for OH and NH stretches by DFT calculations [IEFPCM–DCM solvation]). In addition, none of the peaks in the IR spectrum of 5–H⁺ show widths characteristic of excess protic acid. Finally, as seen for compound 3, DFT calculations also predict that the OH stretch in the *in*-form of 5–H⁺ is blue-shifted by roughly 14 cm⁻¹ compared to the same stretch in the corresponding *out* rotamer.

X-ray Crystallographic Analysis. Single-crystal X-ray analysis of compound 5 reveals an interesting HB network. As hypothesized, the OH group is found exclusively in the inform, thus engaging in a nonconventional hydrogen bond with the adjacent top-aromatic ring and locating the alcoholic proton at 2.108 and 2.237 Å from carbons para and meta to the amino group (predicted 2.074 and 2.213 Å), thus classifying it among the stronger such interactions observed crystallographically. On the other hand, the lone pairs of the OH group readily hydrogen bond to an NH2 group of another molecule (NH···O distance 2.03 Å; N-H distance 0.88 Å). As a result, an extended hydrogen bond network comprised of two conventional (NH···O) and two nonconventional (OH··· π) hydrogen bonds anchors compound 5 in the crystal (Figure 6). Additionally, the carbonyl oxygen on the anhydride ring also engages in a longer-range conventional HB interaction with a neighboring molecule's NH2 hydrogens (NH···O distance 2.245 Å).

Most importantly, the X-ray crystal structure of 5 provided the final missing piece of the crystallographic puzzle. We previously observed that in systems with electron-deficient aromatic rings, the OH group was locked in the *out*-form

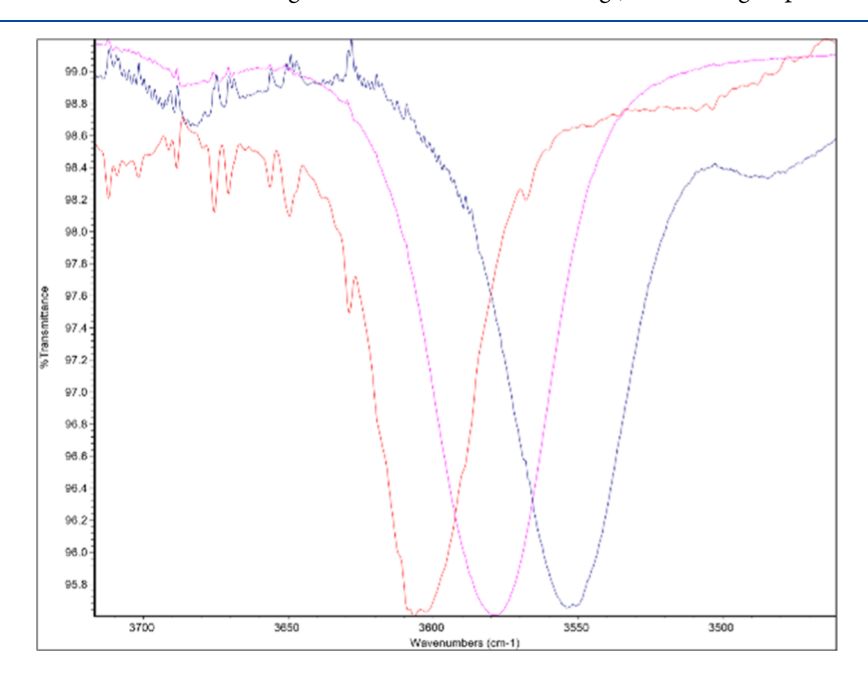


Figure 4. OH region of IR spectra for compounds 1, 3, and 5. Red $(R = CF_3)$; purple (R = H); blue $(R = NH_2)$.

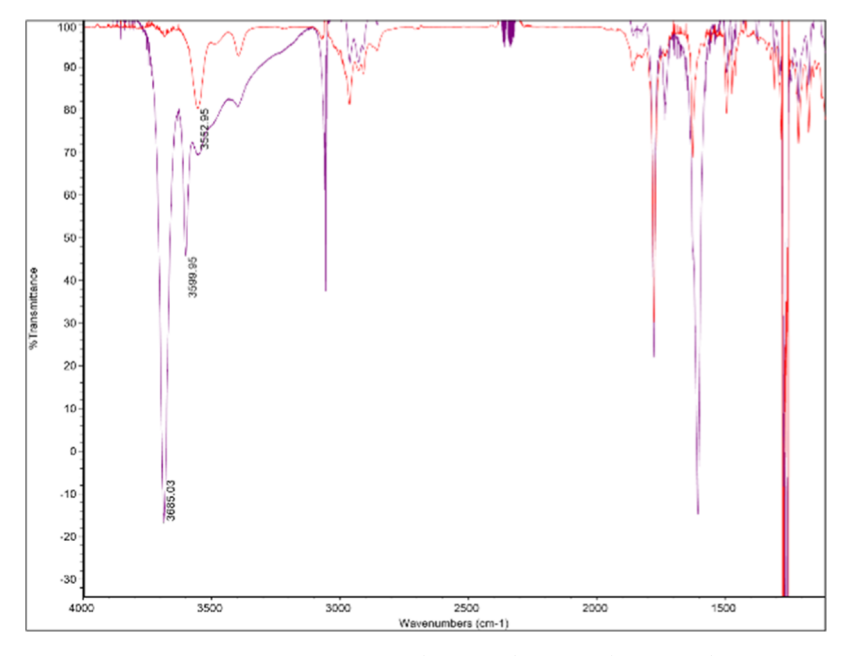


Figure 5. Comparison of IR spectra for compounds 5 and 5-H⁺; red $(R = NH_2)$; purple $(R = NH_3^+)$.

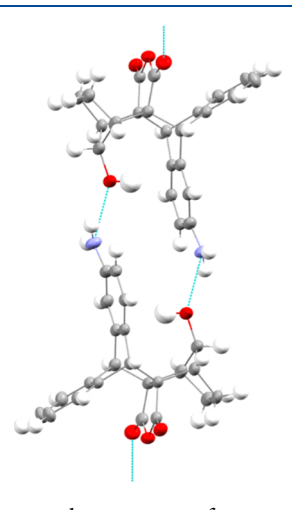


Figure 6. X-ray crystal structure of compound **5** depicting dimerization as a consequence of an extended network of two conventional and two nonconventional hydrogen bonds.

(compound 2), whereas in a nonsubstituted π -system (compound 1), it was partitioned between the *in*- and *out*-forms in the crystal structure.²¹ We observe an electron-rich π -system (compound 5) locking the hydrogen of the OH group in the *in*-orientation, thereby providing a continuous series of crystallographic "snapshots" of a three-stage, tunable system (Figure 7).

Molecular Orbital Interactions. We imagined that a favorable interaction between the aryl-centered π system and OH σ^* MOs can lead to a significant OH··· π hydrogen bond. On the other hand, preferential interaction of oxygen-centered nonbonding "n_o" and aryl-centered π^* MOs can skew the system toward the rotameric HO··· π form. Therefore, we analyzed the relevant MOs in fragments of compounds 1, 3, 5, and $[5-H]^+$ (ω B97XD/6-311+G**). Consistent with chemical intuition, DFT predicts an incremental change in the energies of aromatic ring-centered π and π^* orbitals as the substituents become more electron—donating (Figure 8).

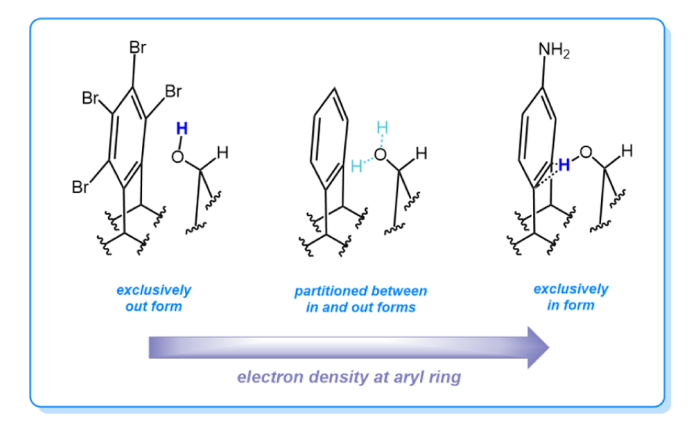


Figure 7. Abbreviated structures of compounds **2**, **1**, and **5** in the solid state showing a stepwise switch from $HO\cdots\pi$ to a nonconventional $OH\cdots\pi$ hydrogen bond.

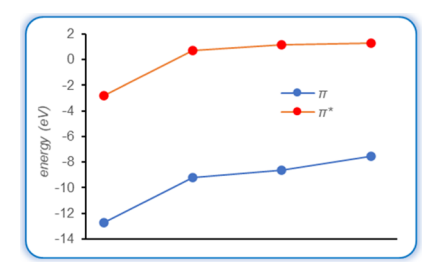


Figure 8. Energies of aromatic-centered highest occupied molecular orbital (HOMO) (π) and LUMO (π^*) ; left to right: $R = NH_3^+$, CF_3 , H, NH_2 .

Additionally, energies of the oxygen-centered n_o and OH σ^* MOs were obtained after optimizing both orientations of the oxygen-bound hydrogen. Interestingly, analysis of charge transfer from an oxygen-based n_o to π^* and aromatic π to OH σ^* reveals that increasing electron density on the aromatic ring lowers the energy gap for the $\pi-\sigma^*$ overlap. This in turn makes OH··· π interactions more favorable, whereas it simultaneously increases the $n_o-\pi^*$ overlap gap (Figure 9).

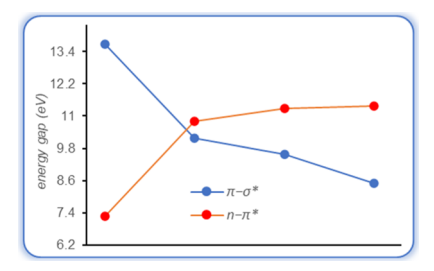


Figure 9. Energy gaps for $n_o-\pi^*$ and $\pi-\sigma^*$ interactions; left to right $R=NH_3^+$, CF_3 , H, NH_2 .

For example, in compound **5**, an aromatic π to OH σ^* interaction is preferred (energy gap = 8.5 eV vs 11.4 eV for n_o to π^*), which locks the system exclusively in the *in*-form. On the contrary, electron transfer from n_o to the aromatic π^* is energetically preferred in **5**–H⁺ (energy gap = 7.3 eV vs 13.7 eV for aromatic π to OH σ^*), thereby favoring the *out*-form (Figures 9 and 10).

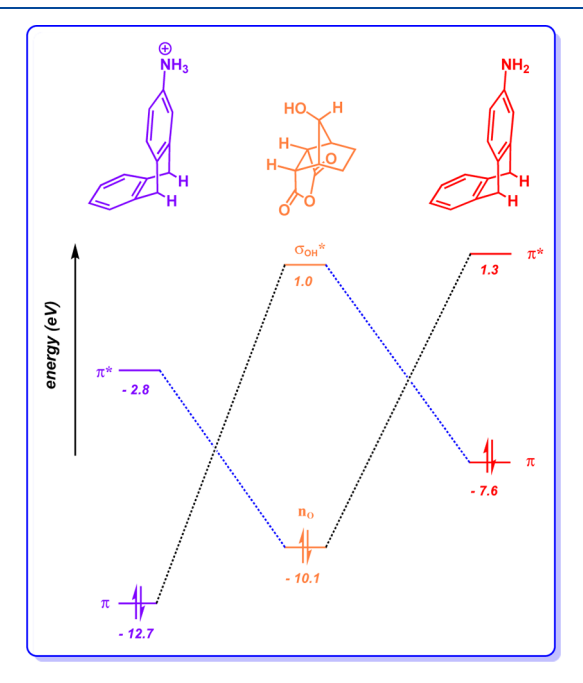


Figure 10. MO diagram representing favorable $n_o - \pi^*$ and $\pi - \sigma^*$ interactions in fragments of $5-H^+$ and $5 (\omega B97XD/6-311+G^{**})$.

Additionally, electrostatic surface potentials (ESP) can provide an alternative explanation because these interactions are largely electrostatic in nature. A negative ESP on the aromatic fragment in 5 attracts the positive region of the OH bond, thereby locking the alcoholic proton in the "in"-orientation. On the contrary, a positive ESP on the aromatic fragment in 5–H⁺ attracts the negative region of the OH containing fragment, thereby reversing the orientation of the alcoholic proton (see Supporting Information for details).

Isodesmic relations comparing the energies of in and out rotamers (Figure 3) can also be explained in terms of the $\pi-\sigma^*$ and $n_o-\pi^*$ overlapping trends observed in Figure 9. For example, $\pi-\text{OH}$ σ^* interactions are dominant in 1 and 5, which pushes the equilibrium toward the in-form, whereas dominant $n_o-\pi^*$ interactions in $5-\text{H}^+$ swing the equilibrium toward the out-form. For 3, however, the two interactions have similar energy gaps (10.2 and 10.8 eV for $\pi-\text{OH}$ σ^* and

 $n_o - \pi^*$, respectively) that keep the equilibrium constant near unity (gas phase).

¹**H NMR Analysis.** We utilized coupling constants between the OH and geminal protons as a qualitative assessment of the extent of OH··· π interactions. The supposition is that stronger OH··· π interactions slow exchange and thereby allow couplings to be measured. In systems with weak or nonexistent OH··· π interactions, more rapid exchange is expected. Experimentally, alcoholic protons in the series appear as doublets with coupling constants of 3.9, 5.4, 7.5, 10.9, and 11.8 Hz in 2, 3, 6 (monobrominated analogue), 1, and 5, respectively (Figure 11). ²¹ Calculations (B3LYP/6-31G(d) and B3LYP/6-311+G-

Figure 11. Chemical shifts of alcoholic protons and their coupling constants in the experimental ¹H spectra of 1, 2, 3, 5, 6, and 7.

(2d,p)) also predict stronger coupling (13–14 Hz for *in*-forms vs 0–6 Hz for *out*-forms, see Supporting Information). As expected, increasing electronic density on the adjacent *top* ring holds the alcoholic proton more tightly because of stronger OH··· π HB; therefore, geminal coupling is observed.

We previously observed that the alcoholic proton in prototype molecule 1 appears fairly shielded (-0.21 ppm) and sharp compared to the *out* diastereomer 7, in which it appears relatively deshielded (1.16 ppm) as a broadened peak. Additionally, the alcoholic protons in 3 and 6 appear some 0.39 and 0.36 ppm deshielded compared to the same proton in $1.^{21}$ Furthermore, the proton geminal to the OH group appears at 3.85 and 2.52 ppm in 1 and its diastereomer 7, suggesting that H···arene interactions experience shielding effects. We attributed these observations to the aromatic ring current effects, that is, reducing H··· π distance shields the interacting proton. We argued that weak OH··· π interactions in 3 and 6 lock the alcoholic proton in the *out*-form; therefore, it is affected by ring current to a lesser extent. ²¹

However, the OH proton of **5** appears at 0.37 ppm, some 0.58 ppm downfield compared to **1**. Calculations (B3LYP/6-31G(d) and B3LYP/6-311+G(2d,p)) predict the alcoholic protons of the *in*-forms to be deshielded compared to the *out*-forms in these molecules, whereas ring current interactions should shield the interacting protons (Table 2, see Supporting

Table 2. Calculated (Scaled) 31 Chemical Shifts of Alcoholic Protons in the *in* and *out* Forms of 1, 3, 5, 5–H⁺, and 6 (B3LYP/6-31G(d)) and the Experimentally Observed Values

¹ H chemical shift	$R = NH_3^+$	CF ₃	Br	Н	NH_2
in-form	2.72	2.72	2.49	2.48	1.52
out-form	0.78	0.95	0.19	0.30	0.46
experimental		0.18	0.15	- 0.21	0.37

Information for details). These effects become apparent in the $^1\mathrm{H}$ spectra as we move from 3 to 6 to 1. In 5, however, hydrogen bond effects dominate and the hydroxyl proton moves back to the positive region of the $^1\mathrm{H}$ spectrum (0.37 ppm, Figure 11). Finally, an outlier is observed in 2 wherein the "alcoholic proton" resonates downfield than 5. The aromatic electron density in this system is probably low enough that the hydroxyl proton is "locked" in the *out*-form. Therefore, it can benefit neither from $\mathrm{OH}\cdots\pi$ HB nor from enhanced ring current effects.

CONCLUSIONS

In this article, we have investigated the effects of an aromatic ring's electronic nature on the strength of $OH \cdots \pi$ HB interactions. Both predicted and experimental IR stretches indicate a direct correlation between the strength of these interactions and the electron density of the π system. The OH stretching frequency red-shifts by roughly 50 cm⁻¹ when the substituent on the aryl ring is modified from CF₃ to NH₂, indicating a significantly stronger HB interaction in the latter case. X-ray crystal structures of various analogues reveal that electron-deficient systems lock the "oxygen-bound hydrogen" in the out-form, whereas electron-rich systems reverse its orientation. Additionally, the crystal structure of top amino analogue 5 reveals an extended hydrogen bond network that effectively dimerizes the system. DFT calculations further suggest that systems with electron-rich aromatic rings show more favorable π -OH σ^* interactions, whereas systems with electron poor aromatic rings depict preferential $n-\pi^*$ interactions. Finally, ¹H NMR analysis reveals that stronger $OH \cdots \pi$ interactions slow exchange of the "alcoholic proton", thereby increasing its coupling constant with the geminal proton. We hope that these results provide additional insights into the significant role of nonconventional HB interactions across a variety of scientific fields.

■ EXPERIMENTAL SECTION

 1H and ^{13}C spectra were acquired on a 400 MHz NMR in CDCl $_3$ at 25 °C, and the chemical shifts are given in parts per million (δ) with respect to an internal tetramethylsilane (δ 0.00 ppm) standard. NMR data are reported in the following format: chemical shifts (multiplicity (s = singlet, d = doublet, t = triplet, q = quartet, m = multiplet, and br = broad), coupling constants [Hz], and integration). IR data were obtained using FT-IR with a flat CaF $_2$ cell.

Synthesis of Compound 4. Compound 1 (180 mg, 0.5 mmol)²¹ was dissolved in 7 mL of CH₃CN, and 80 mg of NH₄NO₃ (1 mmol) in a 3:2 mixture of CH₃CN/TFAA (TFAA = trifluoroacetic

anhydride) was added to the solution. The reaction mixture was stirred at room temperature for 1 h after which the solvent was evaporated under reduced pressure. The mixture was subjected to MPLC separation using hexanes/ethyl acetate as the eluent. The product was isolated as a white solid (185 mg, 82% isolated yield). 1 H NMR (CDCl₃): δ 8.16 (d, J = 2 Hz, 1H), 8.1 (dd, J = 8.1 Hz; 2.1 Hz, 1H), 7.45 (d, J = 8.2 Hz, 1H), 7.27–7.32 (m, 2H), 7.18–7.22 (m, 2H), 4.83 (s, 2H), 4.72 (s, 1H), 2.88 (s, 2H), 1.95–2.1 (m, 2H), 1.55–1.65 (m, 2H); 13 C NMR 1 H 1 (CDCl₃): δ 171.6, 171.5, 147.6, 147.1, 141.8, 139.8, 139.2, 128.34, 128.32, 125.8, 125.6, 123.9, 120.1, 89.7, 67.6, 67.5, 48.7, 48.6, 43.72, 43.67, 24.98, 24.89; IR: 1782, 1649, 1530, 1349 (cm $^{-1}$, CaF $_{2}$, CH $_{2}$ Cl $_{2}$).

Synthesis of Compound 5. To a solution of 4 (150 mg, 0.34 mmol) in 20 mL of EtOH was added 30 mg of Pd/C. The mixture was subjected to hydrogenation in a Parr reactor (3 atm) until 1 H NMR showed complete conversion of 4. The reaction mixture was filtered through a plug of Celite, and the cake was washed with an additional 15 mL of EtOH. The solvent was evaporated under reduced pressure, and the desired product (white solid) was purified by silica gel chromatography using 50% EtOAc in hexanes as the eluent (54 mg, 43% isolated yield). 1 H NMR (CDCl₃): δ 7.19–7.25 (m, 3H), 7.1–7.15 (m, 2H), 6.8 (d, J = 2.3 Hz, 1H), 6.5 (dd, J = 8 Hz; 2.3 Hz, 1H), 4.64 (d, J = 11 Hz, 2H), 3.87 (d, J = 11.4 Hz, 1H), 3.7–3.85 (br, 2H), 2.53 (m, 2H), 1.82 (m, 2H), 1.36 (m, 2H), 0.37 (d, J = 11.7 Hz, 1H); 13 C NMR 1 H 1 (CDCl₃): δ 173.23, 173.17, 146.5, 142.3, 141.3, 140.3, 129.5, 127.7, 127.5, 126.9, 125.4, 125.1, 113.3, 113.2, 85.4, 69.0, 68.6, 48.9, 47.8, 46.19, 46.16, 25.33, 25.29; IR: 3533, 3394, 2963, 2928, 2908, 1778, 1672 (cm $^{-1}$, CaF $_2$, CH $_2$ Cl $_2$).

ASSOCIATED CONTENT

s Supporting Information

The Supporting Information is available free of charge at https://pubs.acs.org/doi/10.1021/acs.joc.0c01121.

Crystal structure of compound 5 (CCDC 1999327) (CIF)

Characterization of new compounds, crystal structure data, and computational information (PDF)

AUTHOR INFORMATION

Corresponding Author

Thomas Lectka — Department of Chemistry, Johns Hopkins University, Baltimore, Maryland 21218, United States; orcid.org/0000-0003-3088-6714; Email: lectka@jhu.edu

Authors

Muhammad Kazim – Department of Chemistry, Johns Hopkins University, Baltimore, Maryland 21218, United States; orcid.org/0000-0003-2020-8952

Liangyu Guan — Department of Chemistry, Johns Hopkins University, Baltimore, Maryland 21218, United States; Calibr—A Division of Scripps Research, San Diego, California 92037, United States

Anant Chopra – Department of Chemistry, Johns Hopkins University, Baltimore, Maryland 21218, United States

Roy Sun – Department of Chemistry, Johns Hopkins University, Baltimore, Maryland 21218, United States

Maxime A. Siegler – Department of Chemistry, Johns Hopkins University, Baltimore, Maryland 21218, United States;
orcid.org/0000-0003-4165-7810

Complete contact information is available at: https://pubs.acs.org/10.1021/acs.joc.0c01121

Notes

The authors declare no competing financial interest.

F

ACKNOWLEDGMENTS

T.L. thanks the National Science Foundation (NSF) (grant CHE 1800510) for financial support.

REFERENCES

- (1) Malone, J. F.; Murray, C. M.; Charlton, M. H.; Docherty, R.; Lavery, A. J. $X-H\cdots\pi$ (phenyl) interactions. Theoretical and crystallographic observations. *J. Chem. Soc., Faraday Trans.* **1997**, 93, 3429–3436.
- (2) Meyer, E. A.; Castellano, R. K.; Diederich, F. Interactions with Aromatic Rings in Chemical and Biological Recognition. *Angew. Chem., Int. Ed.* **2003**, *42*, 1210–1250.
- (3) Burley, S. K.; Petsko, G. A. Amino-aromatic interactions in proteins. FEBS Lett. 1986, 203, 139–143.
- (4) Zheng, H.; Comeforo, K.; Gao, J. Expanding the Fluorous Arsenal: Tetrafluorinated Phenylalanines for Protein Design. *J. Am. Chem. Soc.* **2009**, *131*, 18–19.
- (5) Duan, G.; Smith, V. H.; Weaver, D. F. Characterization of Aromatic–Amide (Side Chain) Interactions in Proteins through Systemic ab Initio Calculations and Data Mining Analyses. *J. Phys. Chem. A* **2000**, *104*, 4521–4532.
- (6) Hughes, R. M.; Waters, M. L. Effects of Lysine Acetylation in a β -Hairpin Peptide: Comparison of an Amide $-\pi$ and a Cation $-\pi$ Interaction. *J. Am. Chem. Soc.* **2006**, *128*, 13586–13591.
- (7) Tóth, G.; Murphy, R. F.; Lovas, S. Investigation of Aromatic-Backbone Amide Interactions in the Model Peptide Acetyl-Phe-Gly-Gly-N-Methyl Amide Using Molecular Dynamics Simulations and Protein Database Search. *J. Am. Chem. Soc.* **2001**, *123*, 11782–11790.
- (8) Ji, X.; Zhang, P.; Armstrong, R. N.; Gilliland, G. L. The Three-Dimensional Structure of a Glutathione S-Transferase from the Mu Gene Class. Structural Analysis of the Binary Complex of Isoenzyme 3–3 and Glutathione at 2.2-Å Resolution. *Biochemistry* **1992**, *31*, 10169–10184.
- (9) Xiao, G.; Liu, S.; Ji, X.; Johnson, W. W.; Chen, J.; Parsons, J. F.; Stevens, W. J.; Gilliland, G. L.; Armstrong, R. N. First-Sphere and Second-Sphere Electrostatic Effects in the Active Site of a Class Mu Glutathione Transferase. *Biochemistry* **1996**, *35*, 4753–4765.
- (10) Sulpizi, M.; Carloni, P. Cation $-\pi$ versus OH $-\pi$ Interactions in Proteins: A Density Functional Study. *J. Phys. Chem. B* **2000**, *104*, 10087–10091.
- (11) Steiner, T.; Koellner, G. Hydrogen Bonds with π -Acceptors in Proteins: Frequencies and Role in Stabilizing Local 3D Structures. *J. Mol. Biol.* **2001**, 305, 535–557.
- (12) Banerjee, P.; Chakraborty, T. Correlation of n_{OH} Spectral Shifts of Phenol-Benzene $O-H\cdots\pi$ Hydrogen-Bonded Complexes with Donor's Acidity: A Combined Matrix Isolation, Infrared Spectroscopy and Quantum Chemistry Study. *J. Phys. Chem. A* **2014**, *118*, 7074–7084.
- (13) Malenov, D. P.; Janjić, G. V.; Veljković, D. Ž.; Zarić, S. D. Mutual influence of parallel, CH/O, OH/ π and lone pair/ π interactions in water/benzene/water system. *Int. J. Comput. Theor. Chem.* **2013**, 1018, 59–65.
- (14) Saggu, M.; Levinson, N. M.; Boxer, S. G. Direct Measurements of Electric Fields in Weak OH $\cdots\pi$ Hydrogen Bonds. *J. Am. Chem. Soc.* **2011**. *133*. 17414–17419.
- (15) Mohan, N.; Vijayalakshmi, K. P.; Koga, N.; Suresh, C. H. Comparison of Aromatic NH $\cdots\pi$, OH $\cdots\pi$, and CH $\cdots\pi$ Interactions of Alanine Using MP2, CCSD, and DFT Methods. *J. Comput. Chem.* **2010**, *31*, 2874–2882.
- (16) Toth, G.; Bowers, S.; Truong, A.; Probst, G. The Role and Significance of Unconventional Hydrogen Bonds in Small Molecules Recognized by Biological Receptors of Pharmaceutical Relevance. *Curr. Pharm. Des.* **2007**, *13*, 3476–3493.
- (17) Motherwell, W. B.; Moïse, J.; Aliev, A. E.; Nič, M.; Coles, S. J.; Horton, P. N.; Hursthouse, M. B.; Chessari, G.; Hunter, C. A.; Vinter, J. G. Noncovalent Functional-Group—Arene Interactions. *Angew. Chem., Int. Ed.* **2007**, *46*, 7823—7826.

- (18) Aliev, A. E.; Arendorf, J. R. T.; Pavlakos, I.; Moreno, R. B.; Porter, M. J.; Rzepa, H. S.; Motherwell, W. B. Surfing π Clouds for Noncovalent Interactions: Arenes versus Alkenes. *Angew. Chem., Int. Ed.* **2015**, *54*, 551–555.
- (19) Paruch, K.; Vyklický, L.; Wang, D. Z.; Katz, T. J.; Incarvito, C.; Zakharov, L.; Rheingold, A. L. Functionalizations of [6]- and [7]Helicenes at Their Most Sterically Hindered Positions. *J. Org. Chem.* **2003**, *68*, 8539–8544.
- (20) Hong, J.; Yang, G.-S.; Duan, C.-Y.; Guo, Z.-J.; Zhu, L.-G. Fluorescence quenching of EB–DNA complex by a novel di-bipyridyl ruthenium(II) complex of p-tert-butyltetrathiacalix[4]arene. *Inorg. Chem. Commun.* **2005**, *8*, 988–991.
- (21) Guan, L.; Holl, M. G.; Pitts, C. R.; Struble, M. D.; Siegler, M. A.; Lectka, T. Through-Space Activation Can Override Substituent Effects in Electrophilic Aromatic Substitution. *J. Am. Chem. Soc.* **2017**, 139, 14913—14916.
- (22) Mataka, S.; Mitoma, Y.; Sawada, T.; Thiemann, T.; Taniguchi, M.; Tashiro, M. Benzo[3.3]benzo[3.3]benzo- and naphtho[3.3]benzo[3.3]naphtho- orthocyclophane bis (alcohol)s. Preparation and structures. *Tetrahedron* 1998, 54, 5171–5186.
- (23) Desiraju, G. R.; Steiner, T. The Weak Hydrogen Bond in Structural Chemistry and Biology; Oxford University Press: New York, 2001.
- (24) Saggu, M.; Levinson, N. M.; Boxer, S. G. Experimental Quantification of Electrostatics in $X-H\cdots\pi$ Hydrogen Bonds. *J. Am. Chem. Soc.* **2012**, *134*, 18986–18997.
- (25) Arunan, E.; Desiraju, G. R.; Klein, R. A.; Sadlej, J.; Scheiner, S.; Alkorta, I.; Clary, D. C.; Crabtree, R. H.; Dannenberg, J. J.; Hobza, P.; Kjaergaard, H. G.; Legon, A. C.; Mennucci, B.; Nesbitt, D. J. Definition of the Hydrogen Bond (IUPAC Recommendations 2011). *Pure Appl. Chem.* **2011**, *83*, 1637–1641.
- (26) Joseph, J.; Jemmis, E. D. Red-, Blue- or No-Shift in Hydrogen Bonds: A Unified Explanation. *J. Am. Chem. Soc.* **2007**, 129, 4620–4632
- (27) Duarte, L. J.; Silva, A. F.; Richter, W. E.; Bruns, R. E. Infrared Intensification and Hydrogen Bond Stabilization: Beyond Point Charges. *J. Phys. Chem. A* **2019**, *123*, 6482–6490.
- (28) Mao, Y.; Head-Gordon, M. Probing Blue-Shifting Hydrogen Bonds with Adiabatic Energy Decomposition Analysis. *J. Phys. Chem. Lett.* **2019**, *10*, 3899–3905.
- (29) Wang, C.; Mo, Y. Classical Electrostatic Interaction is the Origin for Blue-Shifting Halogen Bonds. *Inorg. Chem.* **2019**, *58*, 8577–8586.
- (30) The position of CF₃ group on adjacent top ring was kept identical to the NH₂ analogue for consistency in calculations. However, due to synthetic challenges, the synthesized top CF₃ analogue places the deactivating group on the side position.
- analogue places the deactivating group on the side position. (31) Pierens, G. K. ¹H and ¹³C NMR Scaling Factors for the Calculation of Chemical Shifts in Commonly Used Solvents Using Density Functional Theory. *J. Comput. Chem.* **2014**, *35*, 1388–1394. (32) Brinkley, R. L.; Gupta, R. B. Hydrogen bonding with aromatic
- rings. AIChE J. 2001, 47, 948-953.